Center of pressure plausibility for the double-link human stance model under the intermittent control paradigm

Center of Pressure Plausibility for the Double-Link Human Stance Model Under the Intermittent Control Paradigm

Andrea Tigrini[a], Federica Verdini[a], Sandro Fioretti[a], Alessandro Mengarelli[a,*]

[a]*Department of Information Engineering, Università Politecnica delle Marche, 60131, Ancona, Italy*

Abstract

Despite human balance maintenance in quiet conditions could seem a trivial motor task, it is not. Recently, the human stance was described through a double link inverted pendulum (DIP) actively controlled at the ankle with an intermittent proportional (P) and derivative (D) control actions based on the sway of a virtual inverted pendulum (VIP) that links the ankle joint with the DIP center of mass. Such description, encompassing both the mechanical model and the intermittent control policy, was referred as the DIP/VIP human stance model, and it showed physiologically plausible kinematic patterns. In this study a mathematical formalization of the Center of pressure (COP) for a DIP structure was developed. Then, it was used in conjunction with an intermittently controlled DIP/VIP model to assess its kinetic plausibility. Three descriptors commonly employed in posturography were selected among six based on their capability to discriminate between young (Y) and elderly (O) adults groups. Then, they were applied to assess whether variations of the P-D parameters affect the synthetic COP. The results showed that DIP/VIP model can reproduce COP trajectories, showing characteristics similar to the Y and O groups.

*Corresponding author

Email addresses: a.tigrini@pm.univpm.it (Andrea Tigrini), f.verdini@staff.univpm.it (Federica Verdini), s.fioretti@staff.univpm.it (Sandro Fioretti), a.mengarelli@pm.univpm.it (Alessandro Mengarelli)

Moreover, it was observed that both P and D parameters increased passing from Y to O, indicating that the COP obtained from the DIP/VIP model is able to highlight differences in balance control between groups. The study hence promote the use of DIP/VIP in posturography, where inferential techniques can be applied to characterize neural control.

Keywords: Center of pressure, Upright stance modeling, Human balance maintenance, Intermittent control

---

Word count:

3493

1. Introduction

The study of the human stance received close attention over the years, from biomechanics to neuroscience and robotics (Collins & De Luca, 1993; Peterka, 2000; Popović, 2013), focusing on the comprehension on how the Central Nervous System (CNS) manages the sensory information and how it generates control commands to stabilize the body, eventually preventing falls. Indeed, as experimentally demonstrated, ankle stiffness is not sufficient to guarantee the upright stance stability *per se* (Morasso & Sanguineti, 2002). Thus, a CNS mediated action must come into play to actively support the passive stabilizing mechanisms (Casadio et al., 2005; Baratto et al., 2002; Morasso et al., 2019).

The modeling of the human balance maintenance can be thereby viewed as a cybernetic problem, where the mechanics of the body affects and coexists with the processes that CNS is engaged to solve, i.e. sensory information fusion, motor commands generation and delivery (Morasso et al., 2019). Single-link (SIP) or double-link inverted (DIP) pendulum were commonly adopted to model the body stance (Morasso et al., 2019; Asai et al., 2009; Suzuki et al., 2012; Cenciarini et al., 2010), while the description of the neural controller is currently a discussed topic (Morasso et al., 2019). Many authors approached the problem through a continuous control paradigm, where proportional (P) and derivative (D) controllers act upon a delayed information of the sway angle (Peterka, 2000). This paradigm however presented some limitations, since it is highly sensitive to the feedback loop delay, with poor robust performances. From the other side, the idea that the CNS tunes the regulatory commands (Collins & De Luca, 1993) was further developed and proposed under the variable structure control (VSC) paradigm (Asai et al., 2009; Suzuki et al., 2012; Milton & Insperger, 2019). The latter constitutes a physiologically plausible alternative to a continuous control: through a VSC, the unstable sub-dynamics of the system can be stabilized switching opportunely among them (Asai et al., 2009).

The model proposed by (Morasso et al., 2019) seemed to present a valuable synthesis of the human-balance maintenance. Indeed, the authors modeled the stance through a DIP structure on the sagittal plane, while the neural controller acts at the ankle with an intermittent control policy (Morasso et al., 2019; Asai et al., 2009). The hip instead contributes passively to the stabilization by over-stiffening the upper trunk (Morasso et al., 2019). A crucial point was the idea that CNS employs a delayed knowledge of the Center of Mass (COM) sway to generate active motor commands, leading to the use of a virtual inverted pendulum (VIP) that links the ankle joint to the COM, computed by the position of the DIP structure. Such model showed kinematic coordination patterns between the lower and the upper segments in line with those observed in human balancing (Morasso et al., 2019; Aramaki et al., 2001), resembling actual COM sway. However, no information was provided regarding the Center of Pressure (COP) fluctuations, which together with the COM play a key role in any quiet balancing task (Morasso, 2020). It should be emphasized that the COP time course is a directly measurable quantity, while COM can be only estimated through many possible procedures (Morasso et al., 1999; Cardarelli et al., 2019). Further, classical posturography recognizes COP as fundamental to extract useful information regarding how CNS regulates the stance through the control torques (Collins & De Luca, 1993; Baratto et al., 2002). COP accounts for the resultant control actions exerted not only at the ankle joint but also at the hip. Thus, a SIP model can provide only a limited mechanical description of the human stance.

In this work, a mathematical formulation of COP in the anterior-posterior direction for the DIP model was derived. Then, it was used to assess the plausibility of the DIP/VIP model in reproducing human-like COP balancing patterns, relying on a set of suitable metrics, which require only the anterior-posterior component for their computation. The latter were selected using actual COP data, as descriptive of the underlying mechanisms behind CNS posture regulation (Amoud et al., 2007; Yamamoto et al., 2015; Collins & De Luca, 1993). The active controller parameters of the DIP/VIP were varied within a certain range of values (Morasso et al., 2019). The simulated COP were compared, according to the aforementioned metrics, with actual COP data belonging to two populations, i.e. young and elderly adults, where clear differences in sway patterns were expected.

2. Methods

2.1. Dataset presentation

Posturographic data of thirty healthy subjects from a public dataset were used (Santos & Duarte, 2016), fifteen belonging to a healthy adults group, representing a young cohort (Y) with an age not greater than 36.9 years and fifteen to an elderly group (O), presenting an age greater than 60.0 years. Data were sampled at 100 Hz for 60 s and filtered at 10 Hz with a zero-phase second order low-pass filter and detrended. Only the anterior-posterior component (AP) of COP was considered for further analysis since the DIP/VIP model describes upright posture in the sagittal plane.

2.2. DIP/VIP human upright stance model

The DIP/VIP model describes the human posture through a double link inverted pendulum (see figure 1). Its dynamic equations can be obtained by using the lagrangian formulation (Siciliano et al., 2010; Morasso et al., 2019). The two generalized coordinates q_1 and q_2 (see the appendix) represent the angles between the lower body segment and the vertical axis, and between the lower and upper body segments respectively.

Given $\mathbf{q} = \begin{bmatrix} q_1 & q_2 \end{bmatrix}^T$ one can obtain:

$$\begin{cases} \mathbf{M}(\mathbf{q})\ddot{\mathbf{q}} + \mathbf{C}(\mathbf{q},\dot{\mathbf{q}})\dot{\mathbf{q}} + \mathbf{G}(\mathbf{q}) = \boldsymbol{\tau} \\ \boldsymbol{\tau} = \boldsymbol{\tau}_B + \boldsymbol{\tau}_S + \boldsymbol{\tau}_I + \boldsymbol{\tau}_N \end{cases} \tag{1}$$

where $\mathbf{M}(\mathbf{q})$, $\mathbf{C}(\mathbf{q},\dot{\mathbf{q}})$, $\mathbf{G}(\mathbf{q})$ are the inertia matrix, the generalized Coriolis term, and the gravity dependent torque respectively. The sum of the torques applied at the two joints is represented by $\boldsymbol{\tau}$. More specifically, $\boldsymbol{\tau}_B$ refers to the bias torque, generated by a reference tilt angle between the body and the vertical axis and set to zero (Morasso et al., 2019; Asai et al., 2009; Suzuki et al., 2012). The terms $\boldsymbol{\tau}_S$ and $\boldsymbol{\tau}_I$ refer to the stiffness and intermittent control respectively. The first one is due to the muscles mechanical properties, which passively contribute to the stabilization of the body. Thus, $\boldsymbol{\tau}_S$ was modeled by a proportional and derivative contributes, as highlighted in the following:

$$\boldsymbol{\tau}_S = \begin{bmatrix} K_a q_1 + B_a \dot{q}_1 \\ K_h q_2 + B_h \dot{q}_2 \end{bmatrix} \tag{2}$$

where K_a and K_h model the stiffness at the ankle and the hip. B_a and B_h account for the intrinsic damping properties of the muscles. Instead, $\boldsymbol{\tau}_I$ models the active role of the CNS, since a pure passive mechanical component cannot stabilize human stance (Morasso & Sanguineti, 2002).

In the DIP/VIP modeling framework (Morasso et al., 2019), the novel aspect was to apply the intermittent control only at the ankle joint while the hip coupled the lower body segment passively with the upper trunk, contributing to the stabilization by means of $\boldsymbol{\tau}_S$. Thus, a key element is the use of the VIP model to generate active motor commands. Indeed, for any multi-link mechanical structure, one can obtain the position of the COM, i.e. $x_g(\mathbf{q})$ and

$y_g(\mathbf{q})$ in figure 1 by computing its sway angle q_{COM} (Morasso et al., 2019). The active control $\boldsymbol{\tau}_I$ can be computed following (Morasso et al., 2019; Asai et al., 2009):

$$\boldsymbol{\tau}_I = \begin{cases} \begin{bmatrix} -(P\delta q_{COM} + D\delta \dot{q}_{COM}) \\ 0 \end{bmatrix} & \text{if } \delta q_{COM}(\delta \dot{q}_{COM} - \alpha \delta q_{COM}) > 0 \\ \begin{bmatrix} 0 \\ 0 \end{bmatrix} & \text{otherwise} \end{cases} \tag{3}$$

where δq_{COM} indicates q_{COM} delayed by δ interval of time used to model neural delay, fixed at $\delta = 0.2$ s (Morasso et al., 2019). The intermittent control law applies a proportional and derivative actions at the ankle joint whether COM leaves the stable manifold described by $\delta q_{COM}(\delta \dot{q}_{COM} - \alpha \delta q_{COM}) \leq 0$ (Asai et al., 2009). Here $\alpha = 0.4$ s^{-1} was chosen (Morasso et al., 2019; Asai et al., 2009). Conversely, active control switches off when the system approaches or remains in the stable manifold (Asai et al., 2009). Based on the results presented in (Morasso et al., 2019), in this work P varied between $0.3 \cdot mgh$ and $0.9 \cdot mgh$ N·m, and D between 0 to 200 $N \cdot m \cdot s/rad$ (Morasso et al., 2019).

As reported by (Suzuki et al., 2012; Conforto et al., 2001), quiet upright stance is challenged not only by the gravity field, but also by internal postural noise (Asai et al., 2009; Conforto et al., 2001), represented by τ_N, which acts independently at the two joints. τ_N was modeled as white noise, low-pass filtered at 10 Hz and having standard deviation of 0.2 N·m (Morasso et al., 2019; Suzuki et al., 2012).

2.3. COP formulation for the double link inverted pendulum

Despite the plausibility of DIP/VIP model was assessed in reproducing kinematic human-like sway patterns, no hint regarding the COP time evolution was given (Morasso et al., 2019). In the stance phase (see figure 1) the following equation holds (Chevallereau et al., 2008):

$$m \begin{bmatrix} \ddot{x}_g \\ \ddot{y}_g \end{bmatrix} + mg \begin{bmatrix} 0 \\ 1 \end{bmatrix} = \mathbf{R} = \begin{bmatrix} R_x \\ R_y \end{bmatrix} \tag{4}$$

where m is the total mass of the subject, g is the gravity acceleration, and $\mathbf{R}$ represents the ground reaction force with its two components R_x and R_y. The equilibrium of the DIP around the ankle joint axis can be obtained as:

$$\dot{\sigma}_a = mgx_g - COP(t)R_y - l_a R_x \tag{5}$$

where σ_a is the angular momentum of the DIP about the ankle, COP is the displacement of the center of pressure with respect to the ankle joint and l_a is the height of the latter with respect to the ground (see figure 1). By definition, σ_a is linear with respect to the joint velocities and can be written as reported in (Chevallereau et al., 2008):

$$\sigma_a = \frac{\partial}{\partial \dot{q}_1} \mathcal{L}(\mathbf{q}, \dot{\mathbf{q}}) = \mathbf{N}(\mathbf{q})\dot{\mathbf{q}} \tag{6}$$

σ_a is a conjugate momentum that can be obtained by differentiating the Lagrangian $\mathcal{L}(\mathbf{q}, \dot{\mathbf{q}})$ of the system with respect to $\dot{q}_1$. Such derivative can be rearranged as the scalar product between the vector field $\mathbf{N}(\mathbf{q})$ and the joint velocity vector $\dot{\mathbf{q}}$ (Westervelt et al., 2018) (appendix). Combining (4) and (5), it is possible to compute the COP for a DIP structure:

$$COP(t) = \frac{mgx_g - (\dot{\sigma}_a + ml_a\ddot{x}_g)}{m(\ddot{y}_g + g)} \tag{7}$$

Since the product of l_a and R_x in (5) can be profiled out (Schut et al., 2020), this finally leads to:

$$COP(t) = \frac{mgx_g - \dot{\sigma}_a}{m(\ddot{y}_g + g)} \tag{8}$$

2.4. COP parameters selection and model evaluation

Three COP descriptors were used to assess the kinetic plausibility of the DIP/VIP model. Such descriptors were selected among a set of six, based on their ability in underlining significant differences between the two populations (Y and O). The initial feature set embraced the only two universal indexes in AP direction presented in (Yamamoto et al., 2015): the frequency at which COP presents the 50% (PF50) of its whole power spectrum density (PSD) (Yamamoto et al., 2015; Prieto et al., 1996), and the slope of the PSD in the low frequency band 0.1 - 0.5 Hz (SLOPE-L) (Asai et al., 2009; Yamamoto et al., 2015). Also the critical time (T_{CR}) was included (Toosizadeh et al., 2015; Yamamoto et al., 2015; Novak et al., 2009), obtained as the time interval at which the intersection between the two fitting lines on linear-scale stabilogram diffusion plot (SDP) occurs (Collins & De Luca, 1993). Finally, the generalized Hurst exponent (HE), computed through detrended fluctuation analysis (DFA) (Amoud et al., 2007; Srinivasan et al., 2012), was also considered, together with two features related to sway amplitude, i.e. the mean distance (MD) and the sway range (SR) (Prieto et al., 1996; Błaszczyk et al., 2007). For the DFA computation the windows size ranged from 0.1 s (10 samples) and 10 s (1000 samples). Each feature was computed for both Y and O groups. Normality of data distributions was tested through the Kolmogorov-Smirnov test. Comparisons between groups were performed by ANOVA or Wilcoxon rank sum test for gaussian or non-gaussian distributed data. For each test, statistical significance was set at $p<0.05$.

PF50, T_{CR} and HE resulted able to discriminate between Y and O groups and thus used for the evaluation of COP time-series obtained as output of the DIP/VIP. Such model was implemented in MATLAB/Simulink (The Mathworks Inc.). The anthropometric characteristics required to fill the model were computed as the average among the subjects (appendix). The ranges of values for P and D parameters (section 2.2) were linearly spaced forming a parameter space and used to parametrize the intermittent controller for the simulation of COP from the DIP/VIP model. P-D grids representation was limited to those values for which the model provided stable and physiologically plausible outputs. For each combination of P-D parameters, 10 COP time-series were generated.

Then, PF50, T_{CR} and HE were computed for each COP, providing the dependency of each metric upon P and D combinations. For both groups, it was assumed a plausible range for each considered metric (PMR), defined as the mean population value $\pm$ standard deviation (Table 1). Eventually, a series of grids was built to obtain P and D ranges for which all the three COP descriptors were coherent with synthetic and real data at the same time. Therefore, those P-D values for which the feature maps fell within the PMR-Y and PMR-O at least one time among the ten COP realizations and for all of the three features were selected.

3. Results

The average PSD, represented in a log-log scale (figure 2a) shows a higher power content at the lower frequencies for the Y group and a statistically significant lower PF50 (figure 2b), as confirmed also by the PMR (Table 1).

For Y population, the mean SDP (figure 2c) increased less than the elderly at the lower time scales. This contributes to the higher T_{CR} (Table 1), since the SDP slope in its first part heavily impacts on the T_{CR} estimation (Collins & De Luca, 1993). The statistical analysis (figure 2d) showed significant differences between the groups.

Eventually, the HE exhibited a strong significant difference between the two groups (figure 2f), confirming the discriminant power of this feature (Amoud et al., 2007). This can be appreciated also from the remarkable change in the average regression lines slope between Y and O groups (figure 2e and Table 1).

The three COP descriptors were also computed for the synthetic COP data. Gray-maps (figure 3) describe how PF50, T_{CR} and HE vary with respect to the active control parameterization. PF50 seems to be more sensitive to the variations of D when P was ≈ 300 N·m/rad (figure 3a), and greater PF50 excursions were found for low P values. On the opposite, T_{CR} (figure 3b) seemed to better mirror changes in the P parameter when D was low (between 0 and 50 N·m·s/rad). The HE instead presented a smoothed trend, radially decreasing when both P and D increase (figure 3c). Eventually, the ranges obtained for the two groups were reported in table 2 and their average± standard deviation values are reported as shaded areas in figure 3. Larger P and D values were admissible to obtain COP having characteristics in line with the O group with respect to the Y population. On the contrary, the Y group admitted narrower P and D ranges.

Table 1: Table shows PMR for the three parameters and for both populations.

	PMR		
Group	PF50 (Hz)	T_{CR} (s)	HE
Y	0.09±0.06	1.63±0.59	1.32±0.12
O	0.16±0.13	1.12±0.32	1.17±0.13

Table 2: Table shows the considered P and D ranges for the grids.

Group	P (N·m/rad)	D (N·m·s/rad)
Y	257.36÷322.38	0÷49.47
O	257.36÷463.25	0÷74.21

4. Discussion

The P-D grids (figure 3) seemed to confirm not only the sensitivity of synthetic COP to different parameterizations of the active controller, but also the possibility to obtain time-series whose descriptors lie within the PMR observed in the Y and O groups. This supports the goodness of the DIP/VIP model for the description of the human stance from a kinetic perspective, in addition to the kinematic one (Morasso et al., 2019).

Further, both P and D admitted greater values for the O group compared to the Y one (Table 2). This might indicate the well known functional rearrangement of the CNS control recognized in the elderly (Allum et al., 2002; Collins et al., 1995), which can be mapped through the tuning of the intermittent controller and mirrored by the COP. In passing, greater P and D values were associated with lower HE in the O group (figure 3c). This aspect highlights an enhanced anti-persistent behavior of the elderly, aligning with (Amoud et al., 2007; Collins et al., 1995) and indicating that greater regulatory efforts are needed to achieve stability (Collins et al., 1995), resulting in a more energetically expensive control (Asai et al., 2009).

Regarding the PF50, it quantifies the spreading of the COP spectrum towards the higher frequencies, i.e. the greater is the PF50, the larger is the amount of power of faster dynamics, possibly associated with an augmented level of stochasticity (Yamamoto et al., 2015; Collins & De Luca, 1993). Since

COP encompasses control torques at the lower limbs joints, it undoubtedly reflects also motor commands modulated by muscles activity and their mechanical characteristics (Baratto et al., 2002). Therefore, an enhanced stochastic COP behavior might refer to a "stiffer" muscular strategy, recognizable in the elderly (Collins et al., 1995) and associated either to mechanical muscles properties or to neuromodulatory changes. A global sign of this phenomenon can be found in the PSD slope at the lower frequencies (SLOPE-L) (Yamamoto et al., 2015; Suzuki et al., 2020; Asai et al., 2009): a nearly flat slope points out a body stiffness which tends to be overcritical, i.e. $\gg mgh$, while a negative value stands for an optimal stiffness tuning and thus an efficient regulation (Suzuki et al., 2020; Asai et al., 2009). The former case was associated to a continuous control with higher gains (Asai et al., 2009), while the latter takes advantages from a VSC policy to achieve the global stabilization, admitting lower control gains, resembling a physiological plausible dynamic (Morasso et al., 2019; Suzuki et al., 2020). This agrees with the greater P values for the O population and is also supported by the SLOPE-L computed on the real data of both groups: as expected they resulted higher for the O subjects (-0.95±0.84) with respect to the Y ones (-1.62±1.15).

Eventually, the T_{CR} appears less sensitive to changes in the P-D parameters. From the grids (figure 3b) it is easy to appreciate that T_{CR} has a uniform trend and limited variations for a large set of the controller parameterizations. This aspect is not completely surprising. Despite the DIP/VIP represents a highly descriptive model of the human stance, it naturally incorporates some approximations. Thus, the T_{CR} and the SDP appear able to highlight subtle properties of balance, which might not be necessarily exploited by a mechanistic model, whenever accurate (Baratto et al., 2002). In addition, the SDP represents a conceptual framework for analyzing sway data, grounded on a timeseries perspective rather than on a biomechanical modeling of the system generating COP data (Collins & De Luca, 1993; Baratto et al., 2002). Thus, the role of the T_{CR} in describing VSC models of posture deserves to be further investigated, since it showed to be highly descriptive of different control dynamics exhibited in both healthy individuals and populations presenting a wide spectrum of balance disorders (Toosizadeh et al., 2015; Novak et al., 2009). Note that the choice of a set of COP features already successfully used for investigating COP timeseries in young and elderly subjects (Amoud et al., 2007; Collins et al., 1995; Prieto et al., 1996) further supports the validity of the DIP/VIP model from a kinetic viewpoint. Eventually, it deserves to be mentioned that the active controller parameters investigation was limited to P and D gains, while α was set at a fixed value (Section 2.2). This could represent a partial limitation of the study, since the exploration of α in conjunction with P and D would add significant information regarding the model and thus it needs to be adequately examined in focused studies.

Modern posturography highlighted the tendency to infer active controller parameters to underline differences among many populations or to identify a model for each subject (Suzuki et al., 2020; McKee & Neale, 2019). This is commonly achieved using data or features derived from COM, even if COP measures were the most common data used in classical posturography (Morasso et al., 2019; Suzuki et al., 2012; Morasso, 2020). However, at least a couple of aspects suggest the opportunity to use COP rather than COM. Firstly, COP is a directly measurable quantity, while the COM can only be estimated in a variety of different ways, including the direct computation from COP, which results into a smoothed version of the latter (Morasso et al., 1999; Eng & Winter, 1993). Despite such procedures are commonly employed to highlight kinesiological features of balance, they could lead to a loss of information, that can be instead captured through different identification approaches (Suzuki et al., 2020; Corradini et al., 1997). Indeed, the COP trajectory represents a meaningful source of information regarding both the descending neural control and the mechanical actuation provided by the musculoskeletal system (Baratto et al., 2002), appearing a more preferable choice when human stance is investigated from a neuromuscular perspective. However, the use of a multi-link structure renders more challenging the COP modeling, while defining COP from a single-link inverted pendulum is quite straightforward (Schut et al., 2020). In this view, the relation (8) (section 2.3) can be employed for double-link models. Thus, despite the identification was not the aim of this study, the COP formulation here developed represents itself a valuable contribution toward the integration of physiological data and mechanical models of balance, since the latter provide a high interpretability of its parameters, which can be linked to specific properties of the neuromuscular system.

The additional value of using a DIP/VIP or in general a multi-link model can be appreciated also considering that this allows to investigate if changes in neural control are reflected in how CNS manages the intrinsic body redundancy of the quiet stance (Suzuki et al., 2012; Reimann & Schöner, 2017). Indeed, a loss of the CNS capacity in efficiently managing the redundancy can be a sign of a functional rearrangement due to neurological disorders (Corradini et al., 1997). The central role of COP in accounting for mechanical redundancy is fundamental also in other applications, e.g. bipedal legged robotics. In this context, the COP and more in general the zero moment point has to encompass the multi-link structure in its formulation, in order to properly control both the standing and dynamic phases of gait (Chevallereau et al., 2008; Westervelt et al., 2018). Therefore, an inefficient regulatory activity can be mirrored, and thus recognized, by considering COP characteristics (Peterka, 2009). This could hold also for the human system, where a degraded regulatory activity, due to disease, can affect the multi-link structure management in balance maintenance, which is *per se* a redundant motor task (Reimann & Schöner, 2017).

These aspects support the findings of Morasso et al. (2019), enriched in this study by the kinetic perspective. Present results highlight the suitability of modeling balance through a DIP structure, where VSC accounts for the CNS role. The hybrid policy is employed for managing the body redundancy through the VIP part of the model and resulted to drive synthetic COP characteristics. Indeed, since a physiological coherent model of the control action at the two joints was employed, human-like patterns were observed in the simulated COP time-series. As emerged from (8) and (17), COP spans non linearly the torque vector $\boldsymbol{\tau}$ over σ_a. Thus, both passive and active effects at the hip and ankle were mirrored in the COP, which lumps the information about the stability of the structure.

A further consideration regards the importance of a proper COP modeling, since COP can be used as a feedback information in the balance control loop (Peterka, 2009), rendering the system robust with respect to external perturbations, e.g. support base movements or external impacts (Peterka, 2009; Prahlad et al., 2008). Note that also quiet stance undergoes internal and external disturbance (Conforto et al., 2001; Nomura et al., 2013) and thus COP represents itself a valuable source of information that can be used by the CNS for tuning balance control strategies in either perturbed or unperturbed conditions. Despite one can wonder about the existence of an internal model of the COP within the CNS (Morasso et al., 2019), there is no doubt regarding the existence of an integration process of tactile and proprioceptive sensors of the feet (Viseux, 2020), that makes plausible the existence of COP information within the balance control schemes (Morasso et al., 2019). This suggests a more profound picture regarding the nature of the COP. Indeed, as for certain balancing tasks, CNS must switch the role between COP and COM information in the motor control paradigm (Morasso, 2020). Thus, although classical literature (Winter, 2009) agreed in viewing the COM as the controlled variable and COP as the control variable, it could be a limiting assumption for studying possible rearrangements in the motor control with respect to neurological disorders. This aspect can be further investigated in future studies, where kinematic and kinetic simultaneous measures are available (Santos & Duarte, 2016), in order to better clarify the relationship between COP and COM in this kind of modeling framework.

Appendix

In this section further details regarding the dynamical equation (1), as well as a clarification on the conjugate momentum presented in (6) are shown. Consider the double-link inverted pendulum given in figure 1. By means of Lagrangian formulation, one can easily obtain the matrices required in (1) (Siciliano et al., 2010; Morasso et al., 2019). In particular:

$$\mathbf{M}(\mathbf{q}) = \begin{bmatrix} M_{11} & M_{12} \\ M_{21} & M_{22} \end{bmatrix} \tag{9}$$

$$\mathbf{C}(\mathbf{q}, \dot{\mathbf{q}}) = \begin{bmatrix} C_{11} & C_{12} \\ C_{21} & 0 \end{bmatrix} \tag{10}$$

$$\mathbf{G}(\mathbf{q}) = -g \begin{bmatrix} G_1 \\ G_2 \end{bmatrix} \tag{11}$$

where

$$\begin{cases} M_{11} = I_1 + I_2 + m_1 l_1^2 + m_2(L^2 + l_2^2 + 2Ll_2 \cos q_2) \\ M_{12} = M_{21} = I_2 + m_2(l_2^2 + Ll_2 \cos q_2) \\ M_{22} = I_2 + m_2 l_2^2 \end{cases} \tag{12}$$

$$\begin{cases} C_{11} = -m_2 L l_2 \dot{q}_2 \sin q_2 \\ C_{12} = -m_2 L l_2 (\dot{q}_1 + \dot{q}_2) \sin q_2 \\ C_{21} = m_2 L l_2 \dot{q}_2 \sin q_2 \end{cases} \tag{13}$$

$$\begin{cases} G_1 = (m_1 l_1 + m_2 L) \sin q1 + m_2 l_2 \sin(q_1 + q_2) \\ G_2 = m_2 l_2 \sin(q_1 + q_2) \end{cases} \tag{14}$$

Regarding the conjugate momentum of the DIP with respect to the ankle joint σ_a (equation (6)), it can be obtained differentiating the Lagrangian with respect to the generalized velocity $\dot{q}_1$. Consider the Lagrangian of the mechanical system:

$$\mathcal{L}(\mathbf{q}, \dot{\mathbf{q}}) \coloneqq \mathcal{K}(\mathbf{q}, \dot{\mathbf{q}}) - \mathcal{V}(\mathbf{q}) \tag{15}$$

where the first two terms express the total kinetic and potential energy of the system, respectively (Siciliano et al., 2010; Westervelt et al., 2018). Then, one can observe that only $\mathcal{K}(\mathbf{q}, \dot{\mathbf{q}})$ depends on the generalized velocity $\dot{\mathbf{q}}$. From this, it directly follows that:

$$\sigma_a \coloneqq \frac{\partial}{\partial \dot{q}_1} \mathcal{K}(\mathbf{q}, \dot{\mathbf{q}}) \tag{16}$$

which is convenient since one can observe that:

$$\sigma_a = \begin{bmatrix} M_{11} & M_{12} \end{bmatrix} \dot{\mathbf{q}} = \mathbf{N}(\mathbf{q}) \dot{\mathbf{q}} \tag{17}$$

By differentiating the last equation with respect to time, it follows that the term $\ddot{\mathbf{q}}$ appears in the derivative, which is proportional to the control torques, through the dynamic equation of the DIP (equation (1)). Thus, it follows that all the mechanical fluctuations at the joints are spanned over the COP by $\dot{\sigma}_a$. For supplementary details the reader can refer to (Siciliano et al., 2010; Westervelt et al., 2018). Finally, Table 3 reports the anthropometric characteristics, derived following the relations in (Winter, 2009), of the mean population used to fill the DIP/VIP model.

Table 3: Table shows the anthropometric values used to fill the DIP/VIP model in the simulation steps.

L (m)	l_1 (m)	l_2 (m)	m_1 (kg)	m_2 (kg)	I_1 (kg·m^2)	I_2 (kg·m^2)	K_a (N·m/rad)	K_h (N·m/rad)	B_a (N·m·s/rad)	B_h (N·m·s/rad)
0.87	0.39	0.45	19.3	40.7	2.9	7.9	366.0	246.0	22.0	22.0

Conflict of interest statement

The authors declare that there is no conflict of interest.

References

Allum, J., Carpenter, M., Honegger, F., Adkin, A., & Bloem, B. (2002). Age-dependent variations in the directional sensitivity of balance corrections and compensatory arm movements in man. *The Journal of Physiology*, *542*, 643–663.

Amoud, H., Abadi, M., Hewson, D. J., Michel-Pellegrino, V., Doussot, M., & Duchêne, J. (2007). Fractal time series analysis of postural stability in elderly and control subjects. *Journal of Neuroengineering and Rehabilitation*, *4*, 12.

Aramaki, Y., Nozaki, D., Masani, K., Sato, T., Nakazawa, K., & Yano, H. (2001). Reciprocal angular acceleration of the ankle and hip joints during quiet standing in humans. *Experimental Brain Research*, *136*, 463–473.

Asai, Y., Tasaka, Y., Nomura, K., Nomura, T., Casadio, M., & Morasso, P. (2009). A model of postural control in quiet standing: robust compensation of delay-induced instability using intermittent activation of feedback control. *PLoS One*, *4*, e6169.

Baratto, L., Morasso, P. G., Re, C., & Spada, G. (2002). A new look at posturographic analysis in the clinical context: sway-density versus other parameterization techniques. *Motor Control*, *6*, 246–270.

Błaszczyk, J., Orawiec, R., Duda-Kłodowska, D., & Opala, G. (2007). Assessment of postural instability in patients with parkinson's disease. *Experimental Brain Research*, *183*, 107–114.

Cardarelli, S., Mengarelli, A., Tigrini, A., Strazza, A., Di Nardo, F., Fioretti, S., & Verdini, F. (2019). Single imu displacement and orientation estimation of human center of mass: A magnetometer-free approach. *IEEE Transactions on Instrumentation and Measurement*, *69*, 5629–5639.

Casadio, M., Morasso, P. G., & Sanguineti, V. (2005). Direct measurement of ankle stiffness during quiet standing: implications for control modelling and clinical application. *Gait & Posture*, *21*, 410–424.

Cenciarini, M., Loughlin, P. J., Sparto, P. J., & Redfern, M. S. (2010). Stiffness and damping in postural control increase with age. *IEEE Transactions on Biomedical Engineering*, *57*, 267–275.

Chevallereau, C., Djoudi, D., & Grizzle, J. W. (2008). Stable bipedal walking with foot rotation through direct regulation of the zero moment point. *IEEE Transactions on Robotics*, *24*, 390–401.

Collins, J., De Luca, C., Burrows, A., & Lipsitz, L. (1995). Age-related changes in open-loop and closed-loop postural control mechanisms. *Experimental Brain Research*, *104*, 480–492.

Collins, J. J., & De Luca, C. J. (1993). Open-loop and closed-loop control of posture: a random-walk analysis of center-of-pressure trajectories. *Experimental Brain Research*, *95*, 308–318.

Conforto, S., Schmid, M., Camomilla, V., D'Alessio, T., & Cappozzo, A. (2001). Hemodynamics as a possible internal mechanical disturbance to balance. *Gait & Posture*, *14*, 28–35.

Corradini, M. L., Fioretti, S., Leo, T., & Piperno, R. (1997). Early recognition of postural disorders in multiple sclerosis through movement analysis: a modeling study. *IEEE Transactions on Biomedical Engineering*, *44*, 1029–1038.

Eng, J., & Winter, D. (1993). Estimations of the horizontal displacement of the total body centre of mass: considerations during standing activities. *Gait & Posture*, *1*, 141–144.

McKee, K. L., & Neale, M. C. (2019). Direct estimation of the parameters of a delayed, intermittent activation feedback model of postural sway during quiet standing. *PloS one*, *14*, e0222664.

Milton, J., & Insperger, T. (2019). Acting together, destabilizing influences can stabilize human balance. *Philosophical Transactions of the Royal Society A*, *377*, 20180126.

Morasso, P. (2020). Centre of pressure versus centre of mass stabilization strategies: the tightrope balancing case. *Royal Society Open Science*, *7*, 200111.

Morasso, P., Cherif, A., & Zenzeri, J. (2019). Quiet standing: The single inverted pendulum model is not so bad after all. *PloS One*, *14*, e0213870.

Morasso, P. G., & Sanguineti, V. (2002). Ankle muscle stiffness alone cannot stabilize balance during quiet standing. *Journal of neurophysiology*, *88*, 2157–2162.

Morasso, P. G., Spada, G., & Capra, R. (1999). Computing the com from the cop in postural sway movements. *Human Movement Science*, *18*, 759–767.

Nomura, T., Oshikawa, S., Suzuki, Y., Kiyono, K., & Morasso, P. (2013). Modeling human postural sway using an intermittent control and hemodynamic perturbations. *Mathematical Biosciences*, *245*, 86–95.

Novak, V., Haertle, M., Zhao, P., Hu, K., Munshi, M., Novak, P., Abduljalil, A., & Alsop, D. (2009). White matter hyperintensities and dynamics of postural control. *Magnetic Resonance Imaging*, *27*, 752–759.

Peterka, R. J. (2000). Postural control model interpretation of stabilogram diffusion analysis. *Biological Cybernetics*, *82*, 335–343.

Peterka, R. J. (2009). Comparison of human and humanoid robot control of upright stance. *Journal of Physiology-Paris*, *103*, 149–158.

Popović, M. B. (2013). *Biomechanics and robotics*. CRC Press.

Prahlad, V., Dip, G., & Meng-Hwee, C. (2008). Disturbance rejection by online zmp compensation. *Robotica*, *26*, 9.

Prieto, T. E., Myklebust, J. B., Hoffmann, R. G., Lovett, E. G., & Myklebust, B. M. (1996). Measures of postural steadiness: differences between healthy young and elderly adults. *IEEE Transactions on Biomedical Engineering*, *43*, 956–966.

Reimann, H., & Schöner, G. (2017). A multi-joint model of quiet, upright stance accounts for the "uncontrolled manifold" structure of joint variance. *Biological Cybernetics*, *111*, 389–403.

Santos, D. A., & Duarte, M. (2016). A public data set of human balance evaluations. *PeerJ*, *4*, e2648. doi:10.7717/peerj.2648.

Schut, I., Pasma, J., Roelofs, J., Weerdesteyn, V., van der Kooij, H., & Schouten, A. (2020). Estimating ankle torque and dynamics of the stabilizing mechanism: no need for horizontal ground reaction forces. *Journal of Biomechanics*, (p. 109813).

Siciliano, B., Sciavicco, L., Villani, L., & Oriolo, G. (2010). *Robotics: modelling, planning and control*. Springer Science & Business Media.

Srinivasan, B., Spinner, T., & Rengaswamy, R. (2012). Control loop performance assessment using detrended fluctuation analysis (dfa). *Automatica*, *48*, 1359–1363.

Suzuki, Y., Nakamura, A., Milosevic, M., Nomura, K., Tanahashi, T., Endo, T., Sakoda, S., Morasso, P., & Nomura, T. (2020). Postural instability via a loss of intermittent control in elderly and patients with parkinson's disease: A model-based and data-driven approach. *Chaos: An Interdisciplinary Journal of Nonlinear Science*, *30*, 113140.

Suzuki, Y., Nomura, T., Casadio, M., & Morasso, P. (2012). Intermittent control with ankle, hip, and mixed strategies during quiet standing: a theoretical proposal based on a double inverted pendulum model. *Journal of Theoretical Biology*, *310*, 55–79.

Toosizadeh, N., Mohler, J., Armstrong, D. G., Talal, T. K., & Najafi, B. (2015).

The influence of diabetic peripheral neuropathy on local postural muscle and central sensory feedback balance control. *PloS One*, *10*, e0135255.

Viseux, F. J. (2020). The sensory role of the sole of the foot: Review and update on clinical perspectives. *Neurophysiologie Clinique*, *50*, 55–68.

Westervelt, E. R., Grizzle, J. W., Chevallereau, C., Choi, J. H., & Morris, B. (2018). *Feedback control of dynamic bipedal robot locomotion*. CRC press.

Winter, D. A. (2009). *Biomechanics and motor control of human movement*. John Wiley & Sons.

Yamamoto, T., Smith, C. E., Suzuki, Y., Kiyono, K., Tanahashi, T., Sakoda, S., Morasso, P., & Nomura, T. (2015). Universal and individual characteristics of postural sway during quiet standing in healthy young adults. *Physiological Reports*, *3*, e12329.

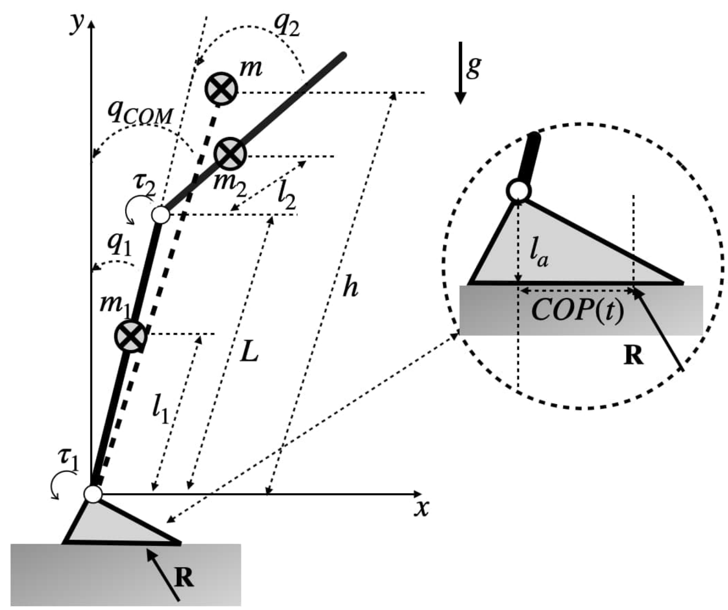

Figure 1: Schematic representation of the human upright stance through a double inverted pendulum (DIP) and its induced single link inverted pendulum model (VIP). The latter virtually links the center of mass COM with the ankle joint.

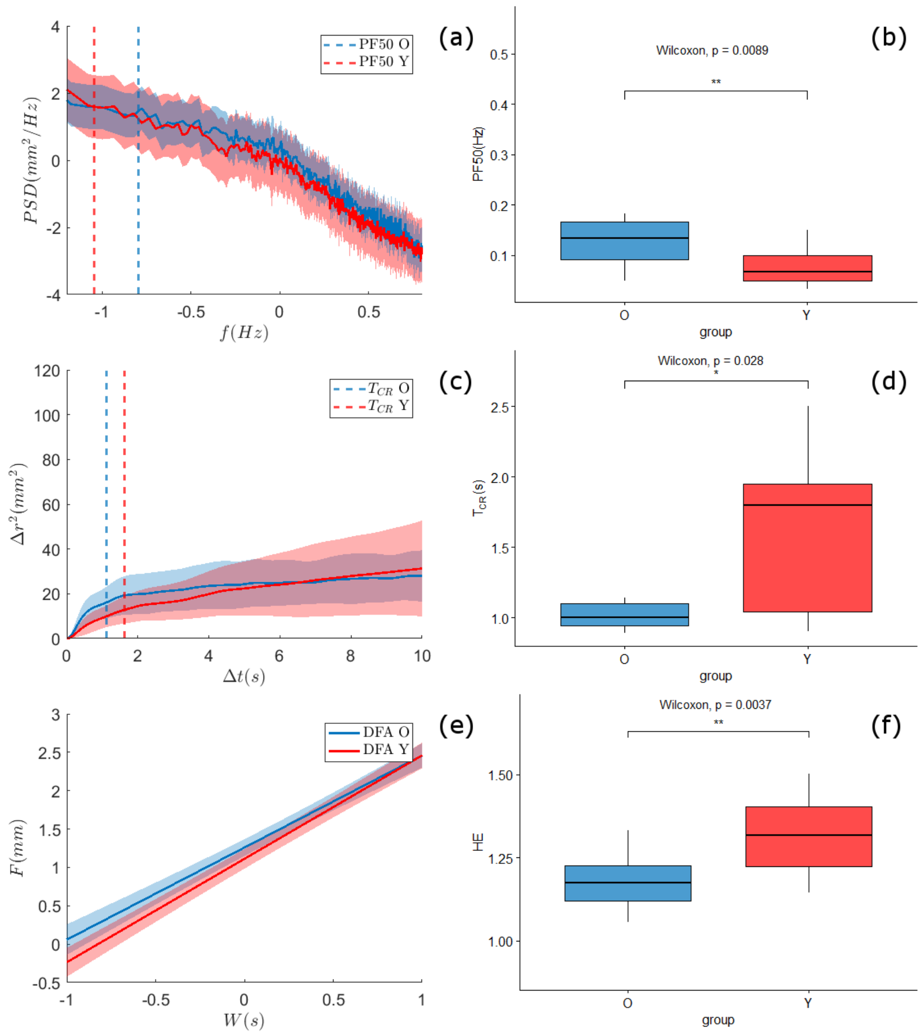

Figure 2: Left panels (2a, 2c) show PSD and SDP averaged values for Y (red) and O (blue) populations. Standard deviations are represented by shaded areas. In panel 2a, vertical dashed lines indicate mean PF50 values for both groups. Vertical dashed lines in panel 2a and 2c represent respectively mean PF50 and mean T_{CR} for Y and O groups. The average regression lines obtained from DFA analysis are presented in panel 2e. Shaded areas stand for the standard deviations. In panels 2a and 2e, both axes are expressed in common logarithmic scale. Right panels (2b, 2d, 2f) show Y (red) and O (blue) groups comparisons for PF50, T_{CR}: and HE. ** indicates $p<0.01$ and * stands for $p<0.05$.

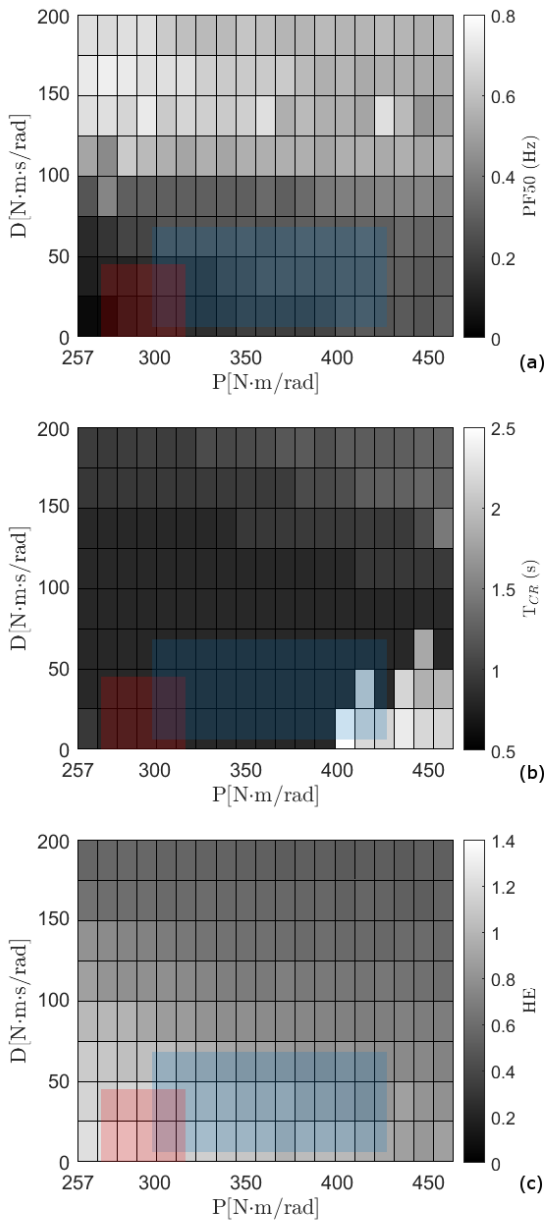

Figure 3: Panel 3a shows how PF50 varied with respect to the P and D parameters. Colormap was obtained computing PF50 from the synthetic COP time-series, obtained for each point of the P-D grid. T_{CR} and HE were computed with the same line and shown in panel 3b and 3c respectively. Shaded boxes, for Y (red) and O (blue) populations, are centered in the average P-D values (289.9 – 24.7 for Y and 360.3 - 37.1 for O), while the areas account for the standard deviation (23.4 – 20.1 for Y and 64.1 – 31.9 for O).